行政院國家科學委員會專題研究計畫 成果報告

鎂鋰合金之成形性研究(重點研究計畫)
研究成果報告(精簡版)

計 畫 類 別 ：個別型
計 畫 編 號 ：NSC 95-2221-E-216-009-
執 行 期 間 ：95 年 08 月 01 日至 96 年 07 月 31 日
執 行 單 位 ：中華大學機械與航太工程研究所

計 畫 主 持 人：吳泓瑜

計畫參與人員：碩士班研究生-兼任助理：周耿中、林家宇、陳宏偉

公 開 資 訊 ：本計畫可公開查詢

中 華 民 國 96 年 10 月 15 日

行政院國家科學委員會專題研究計畫成果報告

鎂鋰合金之成形性研究

Formability Study of Mg-Li Alloy

計畫編號：NSC 95-2212-E-216-009

執行期間：95年 8月 1日至96年 7月31日

計劃主持人: 吳泓瑜　　中華大學機械與航太工程研究所教授

E-mail: ncuwu@chu.edu.tw

計畫參與人員：周耿中、林家宇、陳宏偉　中華大學機械與航太工程研究所研究生

中文摘要

在本計畫中，以單軸拉伸與冲壓成形測試，探討兩種鋰含量鎂鋰鋅合金薄板的機械性能和成形性，以及板片異向性對變形特性的影響。由拉伸測試結果獲得板片的成形性參數；例如平均塑性應變比值、平面異向性和加工硬化係數等。以實驗方式獲得鎂鋰鋅合金薄板的成形極限圖。藉由拉伸實驗數據所獲得的成形性參數，建立了成形性參數與成形極限圖之間的關聯性。冲壓成形實驗樣品的破裂表面以掃描式電子顯微鏡觀察並分析破裂行為。由研究結果顯示，冷軋延的鎂鋰合金薄板片具有明顯的機械性能異向性。LZ90合金的成形性優於LZ60合金。

關鍵詞：鎂鋰合金、異向性、成形性

Abstract

The mechanical property and formability of Mg-Li-Zn alloy thin sheets with two different Li contents have been examined in uniaxial tension and press-forming tests at room temperature. The influence of anisotropy on deformation characteristics was investigated. Formability parameters such as average plastic strain ratio, planar anisotropy, and work hardening exponent were determined by tensile test results. The forming limit diagrams have been experimentally evaluated. The tensile properties and formability parameters were correlated with the forming limit diagrams. The fracture surfaces of the formed samples were examined through use of scanning electron microscope, and the fracture behavior and formability were analyzed. Anisotropic behaviors were observed in the mechanical properties. From the analysis, it was found that formability of the LZ90 alloy was superior compared to that of the LZ60 alloy.

Keywords: Magnesium-lithium alloy; Anisotropy; Formability

1. Introduction

Magnesium is the lightest metal that can be employed in structural applications when alloyed with other elements. Research on Mg alloy focusing on mechanical properties has become very active in the last decade [1-3]. In light of hexagonal close packed (HCP) structure, Mg and its alloys have crucial drawback of poor formability, especially at room temperature, as compared with aluminum and its alloys. Since slip at room temperature is limited to the basal plane, the

processing and forming capabilities of magnesium alloys are generally fairly poor.

Alloying Mg with the lightest metal element, lithium, whose density is 0.534 g/cm^3, yields a Magnesium-Lithium (Mg-Li) alloy with a density similar to that of plastics, and which has only half the density of aluminum alloys. The Mg-Li phase diagram [4] indicates that when the Li content is between ~5.5 and 11.5 wt%, the BCC-structured β phase of the Li solid solution co-exists with the HCP α phase of the Mg solid solution. The β single phase structure could exist for Li contents greater than 11 wt%. As the amount of Li added to the Mg-Li alloy increases, the α phase still possesses HCP structure, but the crystal lattice axes ratio, c/a decreases such that slip between crystal planes become less difficult [5]. The co-existence of the β phase makes the Mg-Li alloy possible to be cold-worked.

The alloy design and mechanical properties of Mg-Li alloys have long been investigated [6-13]. However, the correlation between mechanical properties and formability of Mg-Li alloys has less been examined [6,14], though it is important to the practical use of Mg-Li alloys. In order to examine the possibility of the practical use of Mg-Li alloys, uniaxial tension tests and press-forming tests were performed to explore the mechanical properties, anisotropic behavior and formability of Mg-Li-Zn alloy thin sheets with two different Li contents in the present work.

2. Materials and Experimental Procedures

2.1 Sheet preparation

The Mg-Li alloys were melted in a high-vacuum electric induction furnace under an argon atmosphere. The analyzed chemical compositions of the cast alloys were (wt%) Mg-9.2Li-0.47Zn (designated as LZ90) and Mg-5.8Li-0.46Zn (designated as LZ60). The 200 mm cast cylindrical billets were extruded to a plate with a thickness of 5 mm at a billet preheating temperature of 200°C, and the plates were then cold rolled to a thickness of 0.6 mm.

2.2. Tensile Tests

Uniaxial tension tests were carried out in the directions of 0, 45 and 90° to the rolling direction. The gauge length and width of the tensile specimens were 50 and 6 mm, respectively. The specimens were deformed at room temperature with an initial crosshead speed of 3 mm/min.

The normal anisotropy or average plastic strain ratio ($\bar{r}$) and the planer anisotropy (Δr) were calculated from the r-values (r is the plastic strain ratio which is the ratio of the width strain to the thickness strain) determined along three directions namely parallel (0◦), diagonal (45◦) and perpendicular (90◦) to the rolling direction using the following expressions [15]:

$$\bar{r} = \frac{r_0 + r_{90} + 2r_{45}}{4} \quad (1)$$

$$\Delta r = \frac{r_0 + r_{90} - 2r_{45}}{2} \quad (2)$$

2.3 Press-forming tests

The sheet length for press forming test to determine the FLD was 80 mm with various width. Decreasing the width from 80 to 10 mm causes change in the state of strain from near balanced-biaxial tension through plane strain to uniaxial-tension. The punch speed was kept constant at 6 mm/min during the tests. Grid circles of diameter d_o (2.5 mm) etched on the sheets were used to measure strain levels in each test. During forming the etched circles were distorted into ellipses and/or larger circles, and these deformed grid circles were then used to measure strain levels in each case. Measurements of the major (d_1) and minor (d_2) diameters of the deformed circles after deformation were made to determine the major true strains (ε_1) and the minor true strains (ε_2). The major strains and the minor strains can then be expressed as:

$$\varepsilon_1 = \ln(d_1/d_o) \quad (1)$$

$$\varepsilon_2 = \ln(d_2 / d_o) \quad (2)$$

FLDs were drawn by plotting the minor strain in abscissa and corresponding major strain in ordinate and by drawing a curve which separates the safe region from the unsafe region.

2.4 Metallographic inspection

The specimens for microscopic examination were prepared by conventional metallographic techniques. The polished specimens were etched for 1~5 sec in the etchant of 5 g Picric Acid, 10 ml Acetic Acid, 95 ml Ethyl Alcohol. Optical microscope (OM) was used to examine the microstructures. The fracture surface of the test specimens were analyzed by scanning electron microscope (SEM).

3. Results and Discussion

3.1 Microstructures of the LZ60 and LZ90 alloy

The as-cast structure of the LZ60 alloy presents a dual phase microstructure, as given in Fig. 1(a). β is identified as the Li solid solution of low atomic number while the α phase is the Mg solid solution with a higher atomic number. The as-cast structure of the LZ90 alloy also exhibits a dual phase microstructure including a β matrix plus a distributed α phase in lath form with a width of ~20 μm and a length of ~100 μm, as given in Fig. 1(b). The volume fraction of each phase depends on the Li content, less α phase was observed in LZ90 alloy due to a higher Li content.

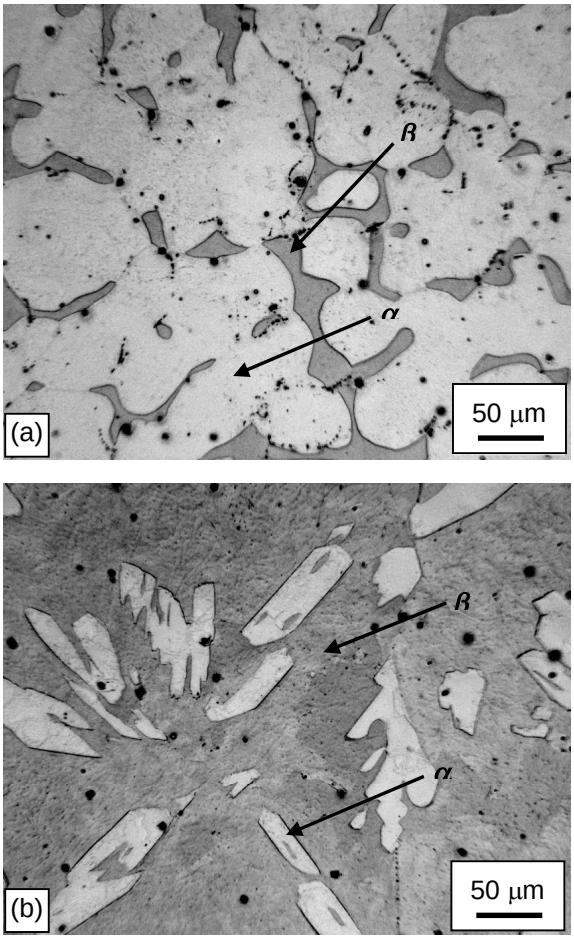

Fig. 1. Optical micrographs of the as-cast microstructures of the Mg-Li-Zn alloys. (a) LZ60, (b) LZ90

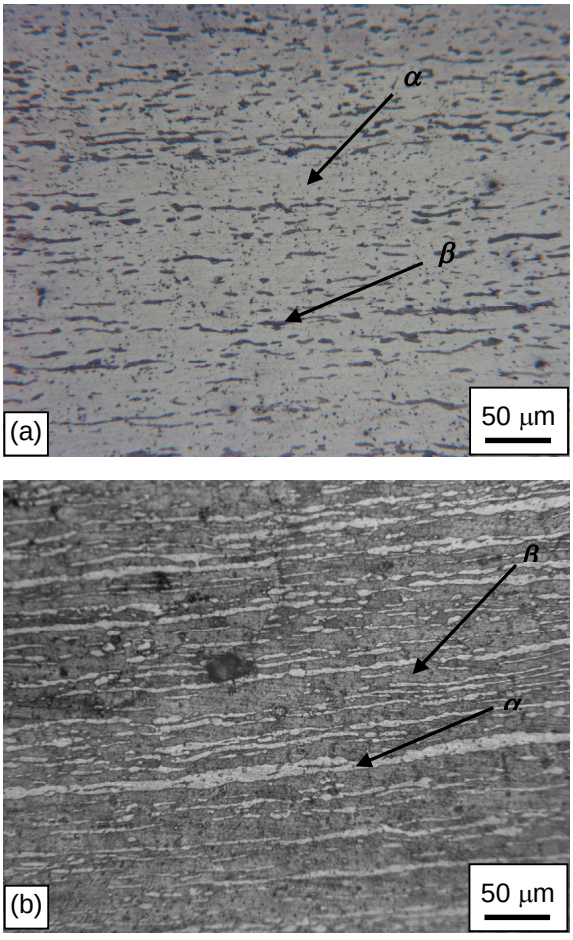

Fig. 2. Optical micrographs of the as-rolled microstructures of the Mg-Li-Zn alloys. (a) LZ60, (b) LZ90

Table 1 Tensile properties of the LZ60 sheet at room temperature

Property	0°	45°	90°	Average
Yield strength (MPa)	126.2	130.2	198.0	146.2
Ultimate tensile strength (MPa)	184.4	188.9	229.2	197.9
Elongation (%)	16.01	28.13	10.28	20.64
Work hardening exponent, *n*	0.213	0.193	0.0357	0.159

Table 2 Tensile properties of the LZ90 sheet at room temperature

Property	0°	45°	90°	Average
Yield strength (MPa)	108.9	114.4	123.6	115.3
Ultimate tensile strength (MPa)	133.0	126.4	135.9	130.4
Elongation (%)	51.9	56.1	43.6	51.9
Work hardening exponent, *n*	0.02144	0.00880	0.00334	0.0106

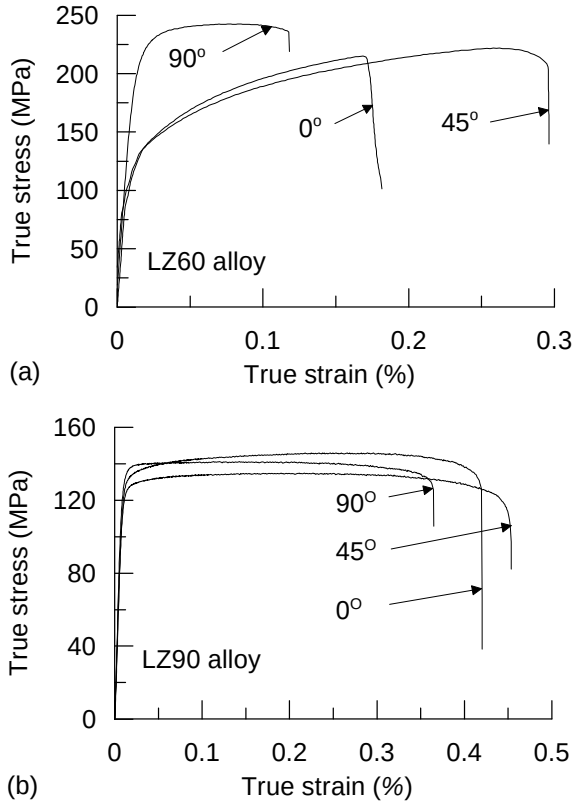

Fig. 3. True stress-strain curves of the Mg-Li-Zn alloys. (a) LZ60, (b) LZ90

Fig. 2 reveals that the as-rolled structures exhibit fibrous rolling texture, which is typical plastically deformed structure. β phase in the LZ60 alloy presents elongated fine strips and dispersed particles in the α matrix, as shown in Fig. 2(a). The morphology of most α phase presented in the LZ90 alloy is coarse long strip, as shown in Fig. 2(b).

3.2 Tensile properties

Fig. 3 demonstrates the true stress-strain curves of the LZ60 and LZ90 alloy in the directions of 0, 45 and 90° to the rolling direction obtained from the uniaxial tension tests with an initial strain rate of 1.67×10^{-3} s^{-1}. The tensile tests were performed on three samples for each direction. The values of the tensile properties for each direction are given in Tables 1 and 2 for the LZ60 and LZ90alloy, respectively. The average values of the strengths, elongation, working hardening exponent are evaluated as [15]

$$\text{Average} = \frac{X_0 + 2X_{45} + X_{90}}{4} \qquad (3)$$

where X is yield strength or ultimate tensile strength, or elongation, or working hardening exponent. Maximum strengths were observed in the 90° direction for both alloys. The elongations in the 45° direction are greater than those in the other directions. The work hardening exponents, *n*, (in the approximation of $\sigma = K\varepsilon^n$), are minima for 90° direction to the rolling direction and maxima along 0° direction. The yield and ultimate tensile strength of the LZ60 are

Table 3 Formability parameters of the LZ60 and LZ90 alloy

Orientation	LZ60		LZ90	
	r	*nr*	*r*	*nr*
0°	1.077	0.229	0.715	0.0153
45°	1.868	0.361	1.419	0.0125
90°	1.525	0.054	0.747	0.0025
average	$\bar{r}$ =1.585	$\bar{n}\bar{r}$ =0.252	$\bar{r}$ =1.075	$\bar{n}\bar{r}$ =0.0114
Δr	-0.57		-0.69	

higher than those of the LZ90 alloy. The elongations in all of the three directions are less than 29% for the LZ60 alloy. The elongations for the LZ90 alloy are comparatively superior, indicated by its elongations in all of the directions greater than 43%. The ductility is quite high owing to the presence of more ductile β phase in the LZ90 alloy.

As reported in the literatures [16-18], when stretching predominates in the forming processes, *n* is the most important factor to influence stretchability. Although the average *n* value of the LZ60 alloy is larger than that of the LZ90 alloy, the average *n* value for the LZ60 alloy is seen to have a low value of 0.159 with an initial tensile strain rate of 1.67×10^{-3} s^{-1}. The LZ60 alloy does not have great elongation and also hasthe low *n* value, therefore the LZ60 alloy might not have good stretchability at room temperature. A rather small average *n* value of 0.0106 was observed for the LZ90 alloy. Although LZ90 alloy shows great elongation, the small value of work hardening exponent reveals that the LZ90 alloy might not be able to present excellent stretchability at room temperature.

3.3. Formability parameters

The formability parameters for the LZ60 and LZ90 alloy determined by experiments are tabulated in Table 3. The normal anisotropy parameter, $\bar{r}$, of the LZ60 alloy is greater than that of the LZ90 alloy due to more HCP α phase presented in the LZ60 alloy. A metal sheet with a larger value of $\bar{r}$ shows a greater drawability [19]. The limit drawing ratio (LDR) is dependent on $\bar{r}$; LDR is the ratio of the largest diameter of the blank that can be drawn without failure to the diameter of the cup or punch. The LZ60 sheet used in this study shows a LDR value of around 1.8 at room temperature. Although the LZ60 alloy presents a $\bar{r}$ value of 1.585, it doe not exhibit good drawability due to a moderate elongation. The planar anisotropy Δr is estimated to have a large negative value of -0.57. A large value of Δr indicates the high earing tendency of LZ60 alloy during drawing operation. Earing is undesirable since more metal must be trimmed.

The LZ90 sheet shows a larger LDR value of 2.0 at room temperature. Although the LZ90 alloy shows a smaller $\bar{r}$ value of 1.075, it gives moderate drawability because of its great elongation. The tendency of ear formation for the LZ90 alloy is still high with a large negative Δr value of -0.69.

3.4. Forming limit diagrams

Fracture limit curves plotted as the forminglimit diagram for the LZ60 and LZ90 alloy from the experimental results are displayed in Fig. 4. In tension-tension region, i.e., biaxial tension region, the limiting fracture major strain is about 14.46% and the limiting minor strain is about 15.66% for LZ60. This shows that the LZ60 sheet of thickness 0.6 mm has limited stretchability in agreement with a low *n* value and moderate elongation. In tension-compression region, the maximum major strain is about 22.41%, the minor strain is about 14.32%. The LZ60 alloy does not

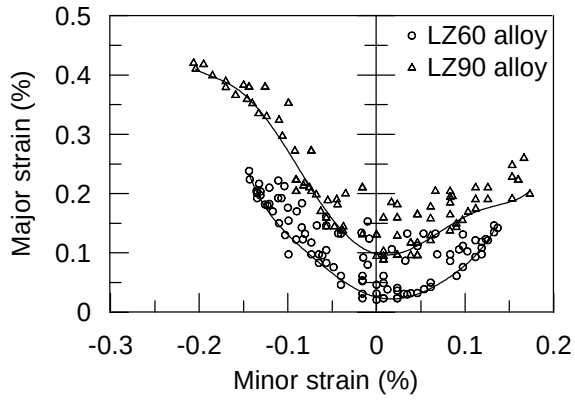

Fig. 4. Forming limit diagrams of the Mg-Li-Zn alloys.

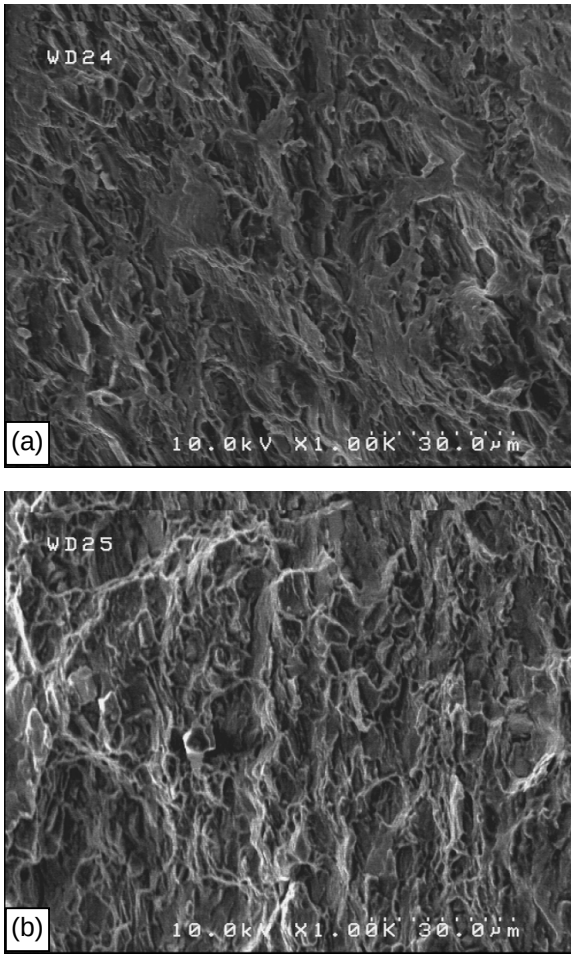

Fig. 5. SEM images of the fracture surface for tension-compression strain condition. (a) LZ60 alloy, (b) LZ90 alloy

present good drawability, in agreement with the low value of LDR. For the near plane strain condition (minor strain = 0), the maximum fracture strain presented a rather low value of about 2.07% only.

In tension-tension region the limiting fracture strains for the LZ90 alloy are higher than those of the LZ60 alloy. The limiting fracture major strain for LZ90 alloy is about 20.17% and the limiting minor strain is about 17.2%. Although the average n value of the LZ90 alloy is much smaller than that of the LZ60 alloy, the greater elongation of the LZ90 alloy gives it a higher stretchability than that of the LZ60 alloy. In tension-compression region, the maximum major strain is about 42.2%, the minor strain is about 20.4%. The LZ90 alloy shows moderate drawability. For the near plane strain condition, the maximum fracture strain presented a low value of about 9.6%.

3.5 Fracture analysis

The SEM images were obtained for the fracture surfaces of the press-forming tests. The samples for SEM observation were cut from the region closet to the origin of the fracture. The various SEM images are demonstrated in the Figs. 5 and 6 for tension-compression and tension-tension strain condition, respectively. For the blanks subjected to tension-compression strain condition, dimpled structure with some flat planes was observed in the LZ60 alloy, as shown in Fig. 5(a). This reveals that the fracture is partly ductile and partly brittle owing to the LZ60 alloy having the HCP α phase matrix, but the ductile fracture is the dominant mode. This result is in agreement with the limiting strains in the tension-compression region of the FLD. Dimpled structure with irregular surface was observed for the LZ90 alloy, as shown in Fig. 5(b), this is the typical fracture surface for ductile fracture.

For the blanks subjected to tension-tension strain condition, the fracture of both alloys appears to be partly ductile and partly brittle, as shown in the Fig. 6, and the evidence for the brittle fracture is more. Some small voids were observed in the LZ60 alloy, as given in Fig. 6(a). In the

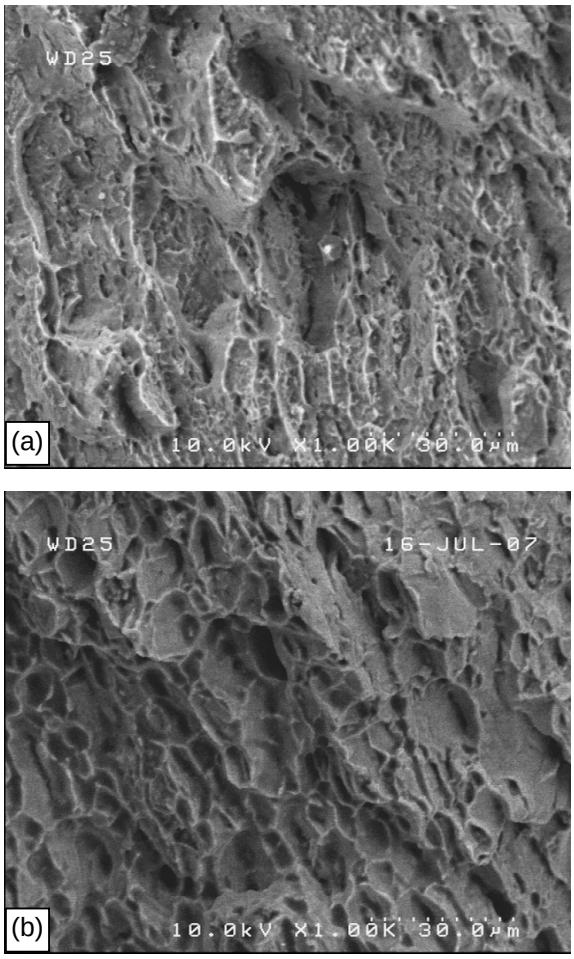

Fig. 6. SEM images of the fracture surface for tension-tension strain condition. (a) LZ60 alloy, (b) LZ90 alloy

LZ60 alloy, elongated fine strips and small particles of β phase are dispersed in the α matrix, as shown in Fig. 2(a). These small voids should be associated with the fine β phase. The fracture features in the tension-tension strain condition are also in agreement with the limiting strains in the FLDs.

4. Conclusions

Mechanical properties and formability of two Mg-Li alloys LZ60 and LZ90 were investigated in this study. The LZ60 alloy exhibited reasonable strength levels and fracture elongation. The LZ90 Mg alloy presented excellent ductility even at room temperature and the strength levels were somewhat inferior. The LZ60 alloy did not exhibited good stretchability and drawability at room temperature. The LZ90 alloy presented better formability than that of the LZ60 alloy. Tensile test results indicated that the $\bar{r}$ value of the LZ60 alloy was not large enough to give good drawability at room temperature. Although the $\bar{r}$ value of the LZ90 alloy was smaller than that of the LZ60 alloy, the greater elongation gave it to present moderate drawability. The large negative values of Δr for both alloys would result in serious ear formation during drawing processes at room temperature. The fracture in the tension-tension strain condition presented partly ductile and partly brittle for both alloys.

Acknowledgments

This work was conducted through grants from National Science Council under the contract NSC 95-2212-E-216-009.

References

[1] Cole GS, Sherman AM. Light weight materials for automotive applications. Mater Characterization 1995;35:3-9.
[2] Kojima Y. Project of platform science and technology for advanced Magnesium alloys. Mater Trans 2001;42:1154-1159.
[3] Haferkamp H, Boehm R, Holzkamp U, Jaschik C, Kaese V, Niemeyer M. Alloy development, processing and applications in Magnesium Lithium alloys. Mater Trans 2001;42:1160-1166.
[4] Nayeb-Hashemi AA, Clark JB, Pelton AD. The Li-Mg (Lithium-Magnesium) system. Bulletin of Alloy and Phase Diagrams 1984;5:365-374.
[5] Herbstein FH, Averbach BL. The structure of lithium-magnesium solid solutions—I: Measurements on the Bragg reflections. Acta Metall 1956;4:407-413.
[6] Takuda H, Matsusaka H, Kikuchi S, Kubota K. Tensile properties of a few

Mg-Li-Zn alloy thin sheets. J Mater Sci 2002;37:51-57.
[7] Takuda H., Enami T, Kubota K, Hatta N. Effect of strain rate on deformation behaviour of a Mg–8.5Li–1Zn alloy sheet at room temperature. Mater Sci Eng A 1999;A271:251-256.
[8] Drozd Z, Trojanová Z, Kúdela S. Deformation behavior of Mg-Li-Al alloys. J Alloys Comp 2004;378:192-195.
[9] Kamado S, Kojima Y. Deformability and strengthening of superlight Mg-Li alloys. Metall Sci Technol 1998;16:45-54.
[10] Saito N, Mabuchi M, Nakanishi M, Kubota K, Higashi K. The aging behavior and the mechanical properties of the Mg-Li-Al-Cu alloy. Scripta Mater 1997;36:551-555.
[11] Agnew SR, Yoo MH, Tomé N. Application of texture simulation to understanding mechanical behavior of Mg and solid solution alloys containing Li or Y. Acta Mater 2001;49:4277-4289.
[12] Crawford P, Barrosa R, Mendez J, Foyos J, Es-Said OS. On the transformation characteristics of LA141A (Mg-Li-Al) alloy. J Mater Process Technol 1996;56:108-118.
[13] Russell AM, Chumbley LS, Gantovnik VB, Xu K, Tian Y, Laabs FC. Anomalously high impact fracture toughness in B.C.C. Mg-Li between 4.2K and 77K. Scripta Mater 1988;39:1663-1667.
[14] Takuda H, Enami T, Kubota K, Hatta N. The formability of a thin sheet of Mg-8.5Li-1Zn alloy. J Mater Process Technol 2000;101:281-286.
[15] Narayanasamy R, Sathiy Narayanan C. Forming limit diagram for interstitial free steels Part I. Mater Sci Eng A 2005;A399:292-307.
[16] Ravi Kumar D, Swaminathan K. Formability of two aluminium alloys. Mater Sci Technol 1999;15:1241-1252.
[17] Mielnik EM. Deep drawing considerations and evaluation of formability. in: Metalworking Science and Engineering, New York: McGraw-Hill, Inc.; 1993, p. 780-792.
[18] Marciniak Z, Kuczynski K, Pokora T. Influence of the plastic properties of a material on the forming limit diagram for sheet metal in tension. Int J Mech Sci 1973;15:789-805.
[19] Ravi Kumar D, Sen A, Swaminathan K. The formability and texture level of a recent automotive stamping grade AI-Mg-Mn alloy. J Mater Sci Lett 1994;13:971-973.

計畫成果自評

本研究依據原計畫目標完成鎂鋰合金性質及成形性的探討，完成之工作項目如下所述：

(1) 超輕鎂鋰合金的擠製及薄板軋延
(2) 鎂鋰合金機械性質的探討
(3) 鎂鋰合金成形參數的探討
(4) 鋰含量對鎂鋰合金機械性質的影響
(5) 鋰含量對鎂鋰合金成形參數的影響
(6) 鎂鋰合金FLD的建立
(7) 成形參數與成形性的關聯性分析
(8) 鋰含量對成形性的影響探討
(9) 應力狀態對破斷模式的影響分析

本計畫完成了鎂鋰合金板片性質與FLD 成形性分析，且完成碩士生研究論文「鎂鋰合金成形性研究」一篇。就研究成果之學術價值而言，適合在國外SCI等級以上之學術期刊發表。研究成果已撰寫論文兩篇，投送中國材料科學學會2007年會發表。投寄於國外學術期刊之論文已撰寫完成，以論文題目 Mechanical and anisotropic behaviors of Mg-Li-Zn alloy thin sheets 投寄國際期刊 Materials and Design，目前正審稿中。

本研究計畫之主要發現，而且也未在其它學術期刊所發表之重要成果包括下列所述之幾項：

1. 鋰元素的添加可以有效地改善鎂合金的延展性，鋰含量越高拉伸延展性越好。含 6 wt%的 LZ60 鎂鋰鋅合金具有合理的強度及延伸率。含 9 wt%的 LZ90 鎂鋰鋅合金強度雖然較 LZ60 合金低，但在室溫狀態下可達到 51.9%的高拉伸延伸率。
2. 鎂鋰合金的冷軋延板材具有明顯的異向性。LZ60 及 LZ90 合金與軋延方向呈 45°試片之延伸率最佳，而與軋延方向垂直試片之抗拉強度最高。
3. 在起始應變速率為 1.67×10^{-3} s^{-1} 的拉伸應變速率下，LZ60 具有少許的加工硬化效應，而 LZ90 合金則沒有明顯的加工硬化效應。由於鎂鋰合金的加工硬化係數小，且加工硬化係數隨鋰元素含量的增加而降低，因而鋰含量會影響鎂鋰合金的成形性。
4. LZ60 合金並未具有足夠大的平均塑性應變比值($\bar{r}$)，所以在室溫狀態無法提供良好的深抽性。雖然 LZ90 合金的平均塑性應變比值較 LZ60 合金為小，但是，LZ90 合金具有相當高的拉伸延伸率。所以 LZ90 合金的深抽性高於 LZ60 合金，其極限深抽比值(LDR)約為 2，與一般的金屬材料；例如鋁合金及不銹鋼等相當。
5. LZ60 與 LZ90 合金的平面異向性值(Δr)均相當大。Δr 值的大小影響深抽過程中皺耳(earing)的形成狀態，皺耳部分在深抽製造的零件中需要被切除而成為廢料。因此，皺耳的產生會影響製造成本。一般而言，希望皺耳的形成是越少越好。然而，LZ60 與 LZ90 合金均具有相當大Δr 值，容易在深抽過程產生皺耳現象。